jpht
www.jpht.info

Journal of Postharvest Technology
2019, **07**(3): 96-114
http://www.jpht.info

RESEARCH ARTICLE

Numerical simulation and experimental validation study of a mixed-mode solar dryer for cocoa beans

Samuel Ayobami Adeyemi[1*], Surajudeen Olarewaju Obayopo[1], Felix Akharume[2]

[1] Thermofluid Research Laboratory, Department of Mechanical Engineering, Obafemi Awolowo University, Ile-Ife, Nigeria.

[2] Department of Biosystems and Agricultural Engineering. University of Kentucky Lexington KY 40506, United States

Received: 05.05.2019 Accepted: 29.06.2019

ABSTRACT

Performance of a mixed-mode solar dryer prototype for cocoa beans was optimized by geometrical optimization of the dryer using numerical simulation. A mixed mode solar dryer was modelled, numerically simulated using computational fluid dynamic (CFD), and the thermal performance of the modelled dryer was experimentally validated for a 50 kg thin layer mass configuration of cocoa beans under no load condition. The simulation parameters include drying chamber cross-sectional area, drying chamber height, drying tray (plenum) position, collector inclination angle as well as velocity of air flow. The simulated results were obtained with reasonable accuracy, and this result showed good agreement with experimental results. In addition, the dryer temperature from experimental validation was higher than that from a similar dryer evaluated by a previous research group from our laboratory. The simulation results show that the dryer performance is optimal at 1 m^2 drying chamber cross-sectional area, 0.2 m drying chamber height and drying tray position placed at a depth 0.1 m from the bottom of the plenum chamber. Also, optimal collector inclination of 14° was obtained. This narrow the analytical-based wide range of collector inclination angle recommended in literatures to $(\alpha - 6.5) \leq \beta \geq (\alpha + 6.5)$ of the earth polar system.

Keywords: CFD modeling; Cocoa beans; Mixed-mode solar dryer.

Citation: Adeyemi, S.A., Obayopo, S.O., and Akharume, F. 2019. Numerical simulation and experimental validation study of a mixed-mode solar dryer for cocoa beans. *Journal of Postharvest Technology*, **7**(3): 96-114.

INTRODUCTION

Solar-assisted drying systems are widely used technique for drying agricultural products in many developing tropical and sub-tropical parts of the world owning to the abundance and availability of solar energy as well as the increasing cost of fossil fuel (Adeniyi et al., 2012; El-Sabaii and Shalaby, 2012). The preference for solar dryers over the traditional open-air sun-dryers is well documented (El-Sabaii and Shalaby, 2012; Jairaj et al., 2009). While open air sun-drying are marred with loss of dried product quality and quantity, resulting from contamination by dirt, dust, unexpected rain, attacks from birds, rodents and other animals; solar drying systems compromise for these challenges by the use of solar collector and drying chamber covered with a transparent glass material, that provides a clean and hygienic environment for the produce being dried and efficiently harnesses the solar radiation for improved quality of dried products.

Based on the mode of operation, solar dryers are typical classified into three groups: direct solar dryers, indirect solar dryers, and hybrid (or mixed mode) solar dryers (Kumar et al., 2016). In direct solar dryers, the sun irradiation is received directly on the produce as it sits in the collector. In indirect systems, the sun irradiation is received by a fluid (air) reservoir that supplies

* *For correspondence:* S. A. Adeyemi (Email: adeyemisamuela@gmail.com)

ISSN: 2348-4330

hot fluid to the drying chamber which houses the produce to be dried. Mixed-mode solar dryers combine the drying mechanism of both the direct and indirect drying system, where drying is done by both direct exposure of produce to solar irradiation and concurrently passing heated air from the heat reservoir through the produce in the drying chamber (Fudholi et al., 2010). Hybrid solar dryer produces better quality dried food at a faster drying rate than other type of dryers due to combined heat sources (Simate, 2003; Singh and Kumar, 2012)

Different designs of solar dryers exist in the market; however, only a few employed numerically designed models. For effective solar drying process, the dimensions and positions of key components of the dryer such as the solar collector, drying chamber, air duct and magnitude of air flow speed require numerical simulation for optimized solar dryer performance (Yadav and Bhagoria, 2013). Most of the published works addressing thermal performance and optimization of the different components of a mixed-mode solar dryer have been limited to the adoption of analytical solutions especially for drying of cocoa beans and other agricultural produce). Fagunwa et al., (2009) developed a hybrid solar dryer for a 50 kg cocoa bean. The dimension and position of the three major components of the dryer were determined analytically; 0.75 x 0.75 x 0.2 m drying chamber dimensions was used based on the bulk density of the cocoa beans, collector's inclination angles of 15° to the horizontal was used based on the earlier works of (Gbaha et al., 2007). Karim, and Hawlader, (2004), also reported a collector's inclination of 10° to the horizontal based on experimental evidence and peculiarity of the meteorological conditions of the test area. In a similar study, Aboul-Enein and research group performed a transient analysis of an inclined flat-plate solar air heater with and without thermal storage using analytical design model (Aboul-Enein et al., 2000). They investigated the effects of collector design dimensions (such as length, width, gap spacing between the absorber plate and glass cover), other design parameters like mass flow rate, thickness and type of storage materials (sand, granite and water) on the outlet and average temperature of the flowing air. They found that with increased length up to 3m and width up to 2 m for a tilted collector as well as an increase in storage thickness up to 0.12 m, the average temperature of flowing air within the dryer increased significantly and consequently increase the heating performance, even till night hours. Jain and Jain (2004) also concluded that the use of tilted solar collectors is even a better contribution to dryer performance than horizontal ones. While analytical approach to the optimization of solar dryers have been widely used in the past, the use of numerical approaches via CFD have proven to provide better results. Ingle et al. (2013) simulated direct solar collector exclusively for grape drying under no-load condition considering temperature distribution and airflow within the dryer. The results obtained from simulation compared with the results obtained experimentally showed good agreement, and it was concluded that CFD simulation is viable tool for solving solar collector problem. In a similar study, Adeniyi et al. (2012) analyzed indirect solar dryer box using ray tracing CFD technique. Temperature distribution and velocity stream within the dryer were simulated without load. The study showed that numerical simulation responds normally to heat effect of solar irradiation. In another study, Maia and co-authors carried out a numerical simulation of the air flow inside an hybrid solar dryer and obtained dryer chamber temperature of 38.45 °C, dryer outlet temperature of 38.15 °C, considering an ambient temperature of 24.05 °C, which was in good agreement with the experimental results of 40.55 °C and 37.85 °C for dryer chamber and outlet temperatures respectively (Maia et al., 2012). Hodali and Bougard (2001), integrated a desiccant unit into a hybrid solar dryer, and thereafter geometrically simulated the drying system for a 15 kg apricot/m^2, their results revealed that the optimized lengths of the collector and drying chamber were 10 and 15 m respectively, while their height and width were identical and equal to 0.1 m and 2 m respectively.

While some works have been done on numerical stimulation of solar dryer, there are death of information on the numerical study of mixed mode solar dryer optimization even so with regards to cocoa beans drying. Additionally, no work was found using computational fluid dynamics to simulate the dimension and inclination angle of this key dryer component and validate effect of thermal performance of the drying chamber and thermal storage. Therefore, the objective of this study was to model

and numerically simulate a mixed-mode solar dryer prototype using computational fluid dynamics, in order to obtain the optimized dimension characteristic of the drying chamber, and the collectors inclination required to achieve optimal performance for drying a 50 kg cocoa beans under no load condition. In addition, we compared the experimentally validated dryer's performance to a previous designed prototype by other researchers within our Laboratory (Fagunwa et al., 2009).

MATERIALS AND METHODS

Numerical procedures

Drying chamber dimension

3D solar model formulation was used to model the three-dimensional structure of the mixed mode solar dryer (figure 1), consisting of a drying unit (drying chamber and plenum chamber) and a symmetrical thermal storage reservoir (housing the collector), aligned together horizontally with the drying unit. Since both the drying unit and thermal storage were symmetric in configuration, the mixed mode dryer was modelled as a single horizontal box (figure 2) and used in the computer simulation. Based on the existing analytical model of Fagunwa's dryer (Fagunwa et al., 2009) and other recommendation in literature, the cross-sectional area of the drying chamber was chosen to range between 0 - 1 m^2 and drying chamber height that ranges between 0-0.5 m were simulated as varied geometry optimization parameters. These ranges agreed with the recommendation of (AusAID, 2010) and other, they recommended the drying chamber ranges between 0 - 1 m^2 surface area to sun irradiation for drying 50 kg of wet cocoa beans.

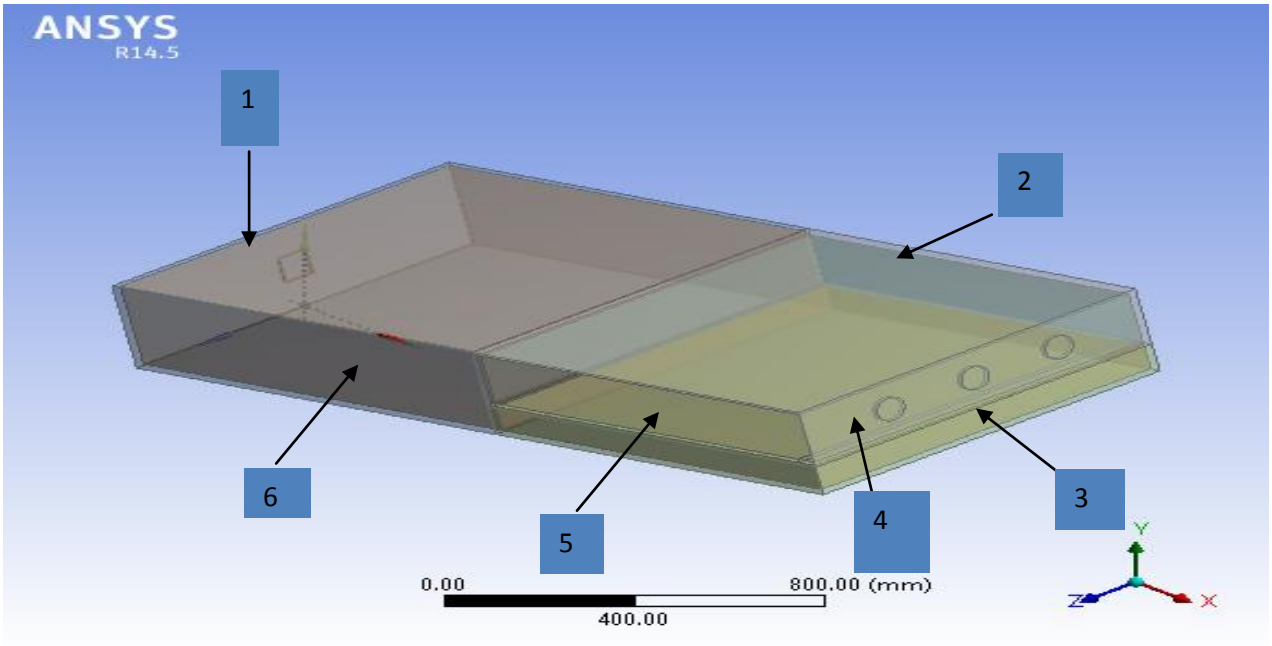

Figure 1. 3-dimensional model of a mixed mode solar dryer. 1- Inlet vent; 2- Plane glass (collector); 3- Air-duct; 4- Outlet vents; 5- Drying chamber; and 6-Thermal storage chamber

Variation of collector's inclination and drying tray position

According to (Gbaha et al., 2007), the optimized angle of solar collector range within (α-10˚) ≤ β ≥ (α +10˚). Where α is the latitude of the research location, and β is the inclination angle of the collector to the horizontal. Since our experimental site (Ile-

Ife, Nigeria) was located on latitude of 7˚ 48', solar collector inclination angle within 0 - 17.5˚ were varied and simulated. The chosen collector inclination values include 0˚, 7.5˚ (latitude of Ile-Ife), 12˚, 13.5˚, 14˚, 15˚, 16.5˚ and 17.5˚. Similarly, to determine optimal air flow speed and position of the drying tray, varied airflow speeds and drying tray positions were varied and simulated. The airflow velocity simulated were free convection, forced convection of 1.2 and 1.5 m/s. while the simulated drying tray position were 0, 0.05, 0.1 0.15 and 0.2 m. The selected airflow velocity was in line with analytical model dryer of (Fagunwa et al., 2009).

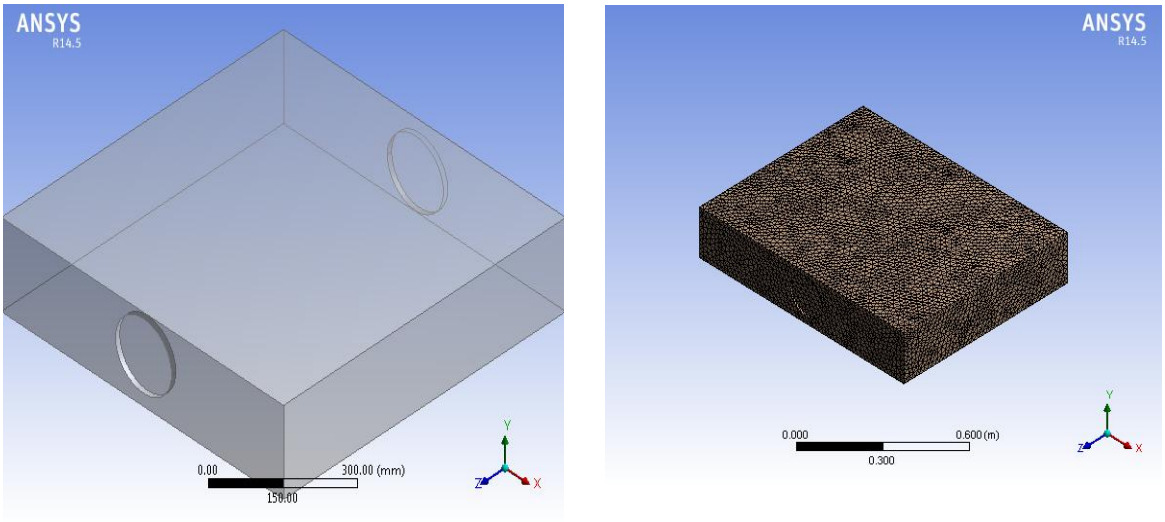

Figure 2. 3D model of the drying chamber (a) without mesh geometries (b) with mesh geometries

Governing equations

The main energy source entering the computational domain through glass is the radiant energy of the sun. 3D segregation solver solves continuity, momentum and energy equations with two extra-transport equations of K-epsilon of turbulent model sequentially. The transport equations for standard K-epsilon model are kinetic energy (K) for turbulence and (∈) turbulent dissipation (Jones & Launder, 1972). The equation for K and ∈ are given in equations 1 and 2 (ANSYSTutorial, 2014). Other turbulence models were tested; K epsilon of viscous model is the one that best fitted the existing experimental data.

$$K = \frac{\partial}{\partial x_j}\left[(\mu + \frac{\mu_t}{\sigma_k})\frac{\partial k}{\partial x_j}\right] + P_k + P_b - \rho \in -Y_M + S_k \quad (1)$$

$$\in = \frac{\partial}{\partial x_j}\left[(\mu + \frac{\mu_t}{\sigma_k})\frac{\partial \in}{\partial x_j}\right] + C_{1\in}\frac{\in}{k}(P_k + C_{3\in}P_b) - C_{2\in}\rho\frac{\in^2}{K} + S_\in \quad (2)$$

The mass, momentum and energy conservation equations are given in equation 3, 4 and 5, respectively. The effect of gravity on heat transport is considered negligible.

$$\frac{\partial p}{\partial t} + \vec{\nabla}.(\rho U) = 0 \quad (3)$$

$$\frac{\partial(\rho U)}{\partial t} + \vec{\nabla}.(\rho U * U) = -\vec{\nabla}p^1 + \vec{\nabla}.\left(\mu_{\text{eff}}(\vec{\nabla}\text{U})\right) + \text{F} \quad (4)$$

$$\frac{\partial(\rho h_{tot})}{\partial t} - \frac{\partial p}{\partial t} + \vec{\nabla}.(\rho U h_{tot}) = \vec{\nabla}.\left(k(\vec{\nabla}T)\right) + S_E \quad (5)$$

The expression for effective viscosity, modified pressure and total specific enthalpy in equations 3 and 4 are given in equations 6, 7 and 8 respectively.

$$\mu_{eff} = \mu + \mu_t \quad (6)$$

$$P = p + \frac{2}{3}\rho k \quad (7)$$

$$h_{tot} = h + \frac{1}{2}U^2 \quad (8)$$

$S_\in$ is the energy equation source term. This term is computed from solar load model of the ANSYS software. In solar load model, energy is computed using solar ray tracing algorithm. In the same model, emissions from surface and the reflecting components of the primary incident load are evenly distributed across all the surfaces. The internal scattered energy which is reflected component of sun's direct irradiation is tracked in the algorithm and area weighted in the solar load computation. The remaining parts of the internally scattered energy are the diffuse solar load contribution by the penetration of the rays through a transparent wall. These values represent the ambient flux when divided by the area of the participating surface.

For optimization purpose, sunny weather with clear skies is assumed. Hence, fair weather condition according to (ASHRAE, 2009) normal direct irradiation is employed. The radiant heat and (ASHRAE, 2009) fair weather condition are given in equations 9 and 10.

$$Q_r = A_s \propto \Delta T^4 \quad (9)$$

$$E_{dn} = I\left\{\frac{\theta}{e^{sinB}}\right\} \quad (10)$$

The absorptivity, reflectivity and transmissivity of the glass boundary that participate in ray tracing algorithm are given as:

$$\alpha_\gamma + \rho_\gamma + \tau_\gamma = 1 \quad (11)$$

The reflectivity is a function of visible light spectral, the absorptivity is a function of direct irradiation components and the transmissivity is a function of the diffuse hemispherical components of incident rays. These functions are respectively expressed as:

$\rho_\gamma = f(\rho_{vd}, \rho_{di}, \rho_{dh})$.

Simulation procedures

3D model of the drying chamber was modeled using ANSYS Fluent Version 14.5, Workbench After 3D modeling, the following steps were followed:

i. The model grid was discretized into cells (meshing) using ANSYS ICEM software as shown in (Fig 2). The total number of elements and nodes were varied for the simulations. The independent meshing operation (called mesh sensitivity) was done as compromise between accuracy and computational expenses. The details of mesh sensitivity were discussed in results and discussion section.

ii. The meshed structures were then imported and simulated in ANSYS FLUENT software. To simulate the temperature distribution within the selected dryers, the prevailing weather conditions for the simulation were set to 13th of 5th month of the year calendar. This was chosen in line with Fagunwa's experimental condition (Fagunwa et al., 2009) for the purpose of validation and comparison.

iii. The physical solving models used in the simulation were 3D segregated solver with steady condition, energy equation, K-epsilon of viscous model and solar load model.

iv. The computations of radiant energy absorbed from solar system were based on latitude 7.4667° N and longitude 4.5667° E of the research location. Therefore, the global solar position of the sun is computed based on this position. Changes in solar time parameters were set at time step 0.1s. The changes were updated through a transient flow at a time step of 0.1 seconds for 10 hours. The computational starting time was 9.00 am of the day. Since research location is located in tropical region, clear sky without cloud condition was employed. So, the sunshine factor is unity. For internal scatter energy, default value of 1423 Wm^{-2} and 200 Wm^{-2} were assumed as a direct solar irradiation and diffuse solar irradiation, respectively. These values described illumination within computational domain.

v. The boundaries conditions used in the simulation for air (simulating fluid), plywood and glass components were shown in Table 1. The air properties used was the prevailing ambient of the research location. The boundary condition for the glass is defined with no slip and the semi-transparent sub model applied at the glass boundary. The glass component of dryer participates in tray tracing algorithm. The wooden parts are defined as adiabatic walls. The vent holes are defined as inlet vent and outlet vent at zero gauge pressure.

vi. The numerical solution was initiated using hybrid initialization method after setting all boundary conditions in fluent software. The solution method adopted was PISO (Pressure Implicit Splitting of operators) algorithm.

vii. The residual monitor was set to visualize the residuals of iterations verses convergence limit.

viii. The numbers of iterations for final results were set around 10,000. The results for these simulations converged at around 1800 to 4000 iterations.

ix. After getting the proper converged results, the temperature distributions inside the drying chamber were plotted in the form of Contour plots.

x. The average temperatures within simulated drying chamber were calculated.

Table 1. Boundary conditions used in the simulation process for air, plywood and glass

Property	Air	Plywood	Glass
Density (kg/m^3)	166	545	2500
Specific Heat (J/kg K)	1005	0.122	720
Thermal Conductivity (W/m K)	0.0264	0.12	1.05
Thickness (mm)	-	12	4
Transmissivity	-	-	0.90
Viscosity (kg/m-s)	1.604 x 10^{-5}	-	-

Source: (Engineering_ToolBox, 2003)

Experimental validation

Design Consideration

The optimal dimension of the drying chamber was based on the result of the numerical simulations considered to dry a 50 kg cocoa beans. The drying unit, consisting of a drying chamber and plenum chamber, was designed as a rectangular box of dimension 1 m x 1 m x 0.3 m, with a drying tray of dimension 1 m x 1 m sitting at a depth 0.2 m from the top of the drying chamber, leaving a plenum of 0.1 m height, such that the air duct of diameter 0.08 m sits centrally in the plenum chamber. For validation and comparison, the dimension of the solar collector was based on bulk volume of agricultural produce (cocoa beans). The useful energy gain by solar collector was estimated by Hottel-Whiller's equation (equation 12) and heat removal factor (F_r) by equation 13 (Gatea, 2010).

$$Q_u = A_c F_r[(\alpha\tau)\mathrm{I_T} - U_l(T_c - T_a)] \quad (12)$$

$$F_r = \frac{mc_p(T_c - T_a)}{A_c[(\alpha\tau)\mathrm{I_{tot}} - U_l(T_c - T_a)]} \quad (13)$$

The thermal efficiency of the dryer is given as

$$\eta = \frac{\mathrm{Q_u}}{\mathrm{I_T A_c}} \quad (14)$$

According to (Gatea, 2010)**,** the effective collector area is given as

$$A_c = \frac{\dot{m}c_p(T_c - T_D) + \dot{\mathrm{M}}\mathrm{L}}{F_r[(\alpha\tau)\mathrm{I_T} - U_l(T_D - T_a)]} \quad (15)$$

The useful energy of the collector delivers to the drying chamber per unit time is given as

$$Q_u = \dot{m}c_p(T_c - T_D) + \dot{\mathrm{M}}\,\mathrm{L} \quad (16)$$

The quantity of the granite stones coated with coal-tar in thermal chamber and the volume coal-tar granite stones (V) are given in equation 17 and 18 respectively (Markatos, 1983).

$$\frac{T_c - T_a}{T_d - T_a} = e^{\left(\frac{-hA}{\rho cv}\right)t} \quad (17)$$

$$\mathrm{V} = \frac{hA\,t}{cv\ln\left(\frac{T_c - T_a}{T_{D-T_a}}\right)} \quad (18$$

The dryer description

the major components of the dryer include a thermal storage chamber (with collector and absorber), and the drying chamber. a schematic view of the dryer is shown in (figure 3a) while the experimental dryer is shown in (figure 3b). the length of the dryer was placed in north-south direction for even distribution of solar heat flux from both wings of solar travelling directions (east-west) (ausaid, 2010). the upper part of the mixed mode dryer consists of drying chamber and an air-duct. the air-duct is located at the lower part of the drying chamber (plenum) with a diameter of 0.08 m from the drying tray (made of stainless wire mesh) and the bed of the drying chamber. the drying system is covered with a 0.004 m thick transparent glass for easy penetration of the solar irradiation and sealed to prevent heat loss**.**

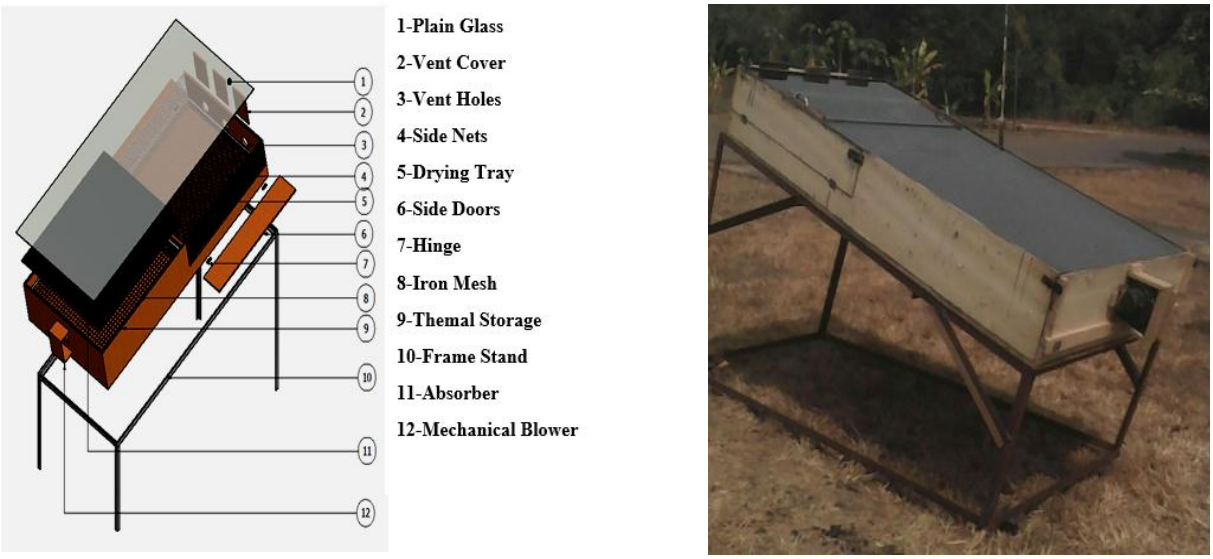

a b

Figure 3. Schematic and experimental diagram of the mixed-mode solar dryer (a-schematic view, b-experimental dryer)

The air-duct creates warm air density gradient between thermal storage and drying chamber, hence, natural convection is easily achieved within the dryer. The thermal storage chamber comprises layers of granite stones coated with coal-tar. Four layers set of coal-tar coated granite stones, each of thickness of 50 mm were laid with a 15 mm gap between each stone to ensure proper venting of hot air. A 2 mm thick galvanized iron plate coated with coal-tar sits directly on the layer of stones (absorber). Mechanical blower was mounted at lower end of the thermal chamber only for the experiment to test the effect of forced convection on thermal performance of the dryer at different airflow speed. The whole mixed-mode solar drying unit was set at an inclination angle of 14˚ for optimum irradiation.

Measured parameters

The dryer was evaluated for optimal performance without loading. Additionally, numerical simulations and experimental investigations were carried out to study the temperature distribution for the dryer on hourly basis. Readings of air temperature were taken at three different points inside drying chamber, and the corresponding solar intensity for different hours of the experiment were recorded. Each reading was observed three times and average the readings were reported. Type K data logger S220 thermocouple was used in measuring the air temperature in the dryer. The experiment started at 8 am of the 27th of January 2016 and each test run lasted for 9 hrs.

RESULTS AND DISCUSSION

Drying chamber dimension optimization

Mesh sensitivity

The number of elements and nodes of grid independent tests, ranging between 106,785 elements and 21,340 nodes were observed. The control parameters for the grid independent tests were the average air-temperature inside and at the exit of the simulated chamber as shown in Table 2.

Table 2: Mesh Sensitivity of modelled drying chamber

Mesh	Node number	Drying air temperature (°C)	Outlet air temperature (°C)
1	18200	36	34
2	18900	38	35
3	19100	45	42
4	20200	48	39
5	20900	48	43
6	21000	48	43
7	21340	48	43

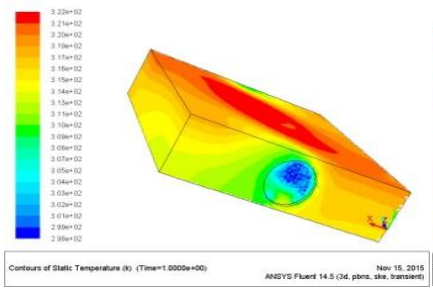

A: 0.75 m × 0.75 m × 0.2 m

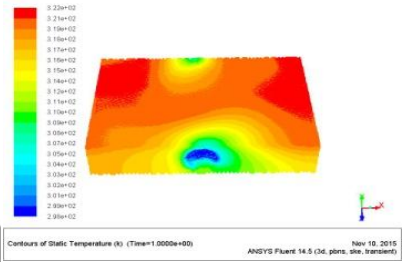

B: 1 m × 0.7 m × 0.2 m

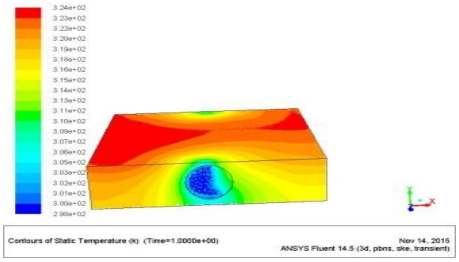

C: 1 m × 0.8 m × 0.2 m

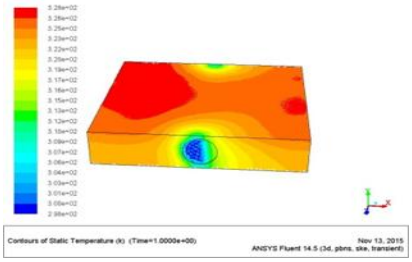

D: 1 m × 0.9 m × 0.2 m

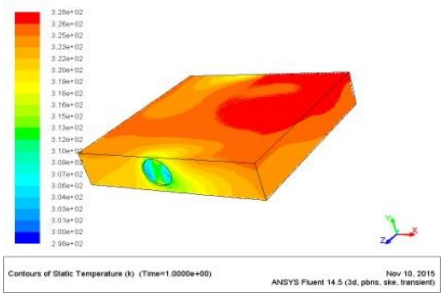

E: 1 m × 1 m × 0.2 m

Figure 4. Temperature distribution contours within different drying chamber dimensions using varied surface area

Effect of dimension optimization on temperature distribution within the drying chamber

The heat contours of temperature distribution are shown in (figure 4). It can be observed that the air near the tranparent glass cover posseses highest temperature. This reveals the direction of solar radiation and subsequently proves that only the glass material contributes majorly to the ray tracing algorithm and not the other components since the other components are opaque and adiabatic walls. The low temperature at inlet and outlet vent reveals the convective cooling effect of the incoming ambient air to the drying chamber. The average chamber temperature across the different simulated drying chamber crossectional area is presented in fiure 5. It can be observed that the temperature within drying chamber increases with increase in expose cross-sectional surface area to the sun. A typical temperature increament of about 3 ˚C was recorded for every 0.1 m^2 increament. Based on this analysis, drying chamber with dimension 1.0 m $\times 1.0\, m$ was selected as optimum drying chamber area for drying 50 kg of cocoa beans. Similar dimension range was recommended by (AusAID, 2010) for drying 50 kg cocoa beans (AusAID, 2010).

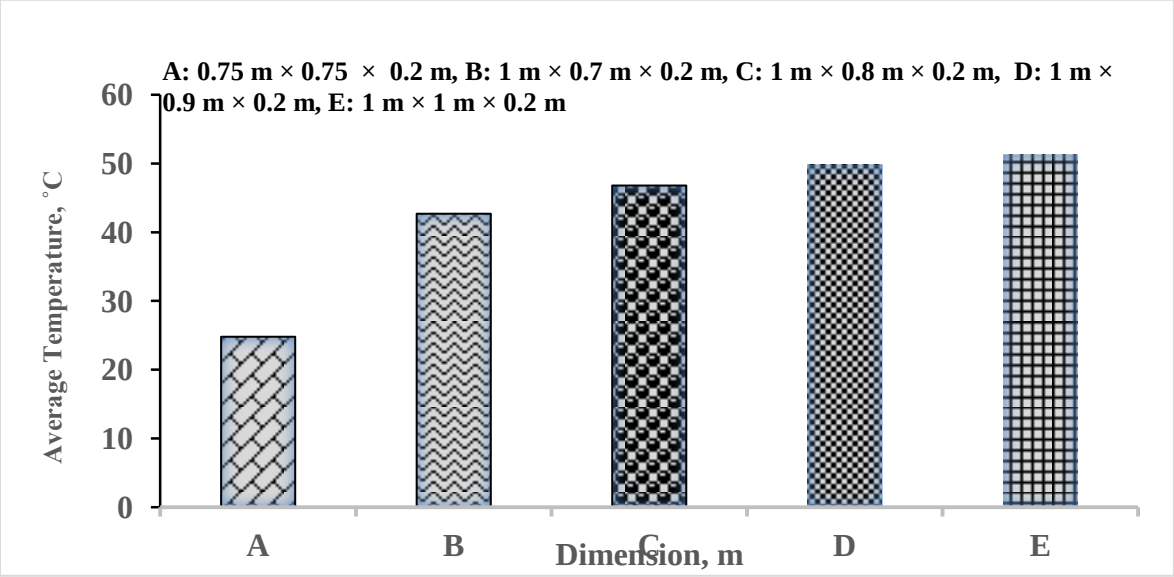

Figure 5. Average temperature within varied drying chamber surface area

Having determined the optimal drying chamber cross sectional area at thermal point good enough for drying cocoa beans and other agricultural produce, the height of the chamber (space above the plenum) was simulated, within the chosen the crosectional area. The heat contours of temperature distribution with reference to drying chamber height are presented in figure 6 while the average drying chamber temperature is presented in figure 7. From figure 6 and 7, it can be seen that air temperature within drying chamber decreases with increase in drying chamber height. A typical temperature decrease of about 1.5 ˚C was recorded for every 0.1 m increament in height. Drying chamber of 1 m × 1 m × $0.2\, m$ was selected as optimum height based on the average air temperature. Also, a lower air temperature was observed at inlet and outlet vent of the chamber compare to corresponding temperature in the dryer. This was due to convective cooling effect of the ambient air. However, the outlet air temperature from the dryer increases with increase surface area and decreases with increase in drying bed. Similar results were reported on thermal analysis of solar air heaters for drying purposes (Amer et al., 2010; Karim & Hawlader, 2004).

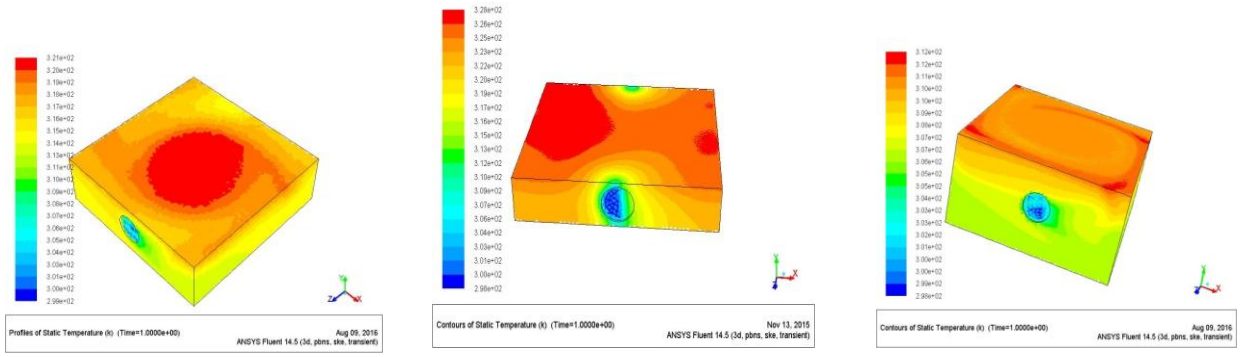

1m× 1 m × 0.3 m 1 m × 1 m × 0.4 m 1 m × 1 m × 0.5 m

Figure 6. Contours of temperature variation within varied drying chamber height

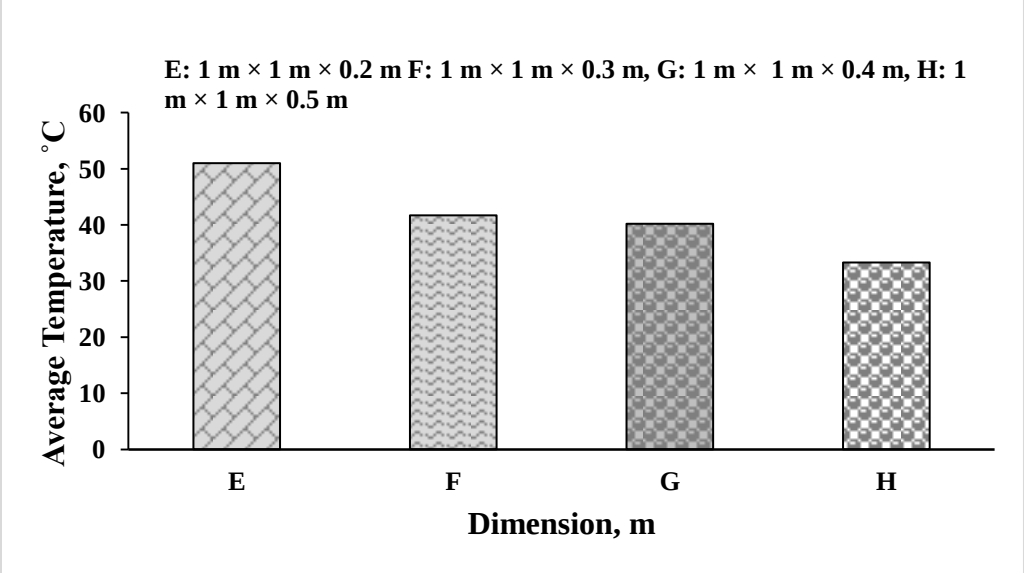

Figure 7. Average temperature within varied drying chamber height.

Effect of tray position on temperature and drying air distribution

To determine the optimal position of the drying tray within the drying unit, stack of drying trays were simulated and the simulated drying positions were 0, 0.5, 0.1, 0.15 and 0.2 m. Free convection was considered for the simulation in line with the previous work of (Fagunwa et al., 2009). Figure 8 shows degree of temperature and airflow distribution at different positions of the drying tray. From the figure 8a., the solar irridation received by the tray decreases with increasing tray depth within the drying chamber. However, a uniform temperature distribution was observed at various level of the tray position. The contours in figure 8b revealed even distribution of airflow across the tray positions. However, the effect of inlet and outlet vent was visibly noticed at tray position 0.1 and 0.15 m. Therefore, drying tray was position at 0.1 m from the bottom of plenum chamber for optimal performance.

Airflow pathline of free and forced convection are shown in figure. 9. Uniform and well define directional trajectory of airflow are observed within the simulated dryer irrespective of free and forced convection methods adopted. However, the intensity of

the airflow pathline varied with increase in airflow speed. Hence, free convection is recommended in this work in line with (Fagunwa et al., 2009).

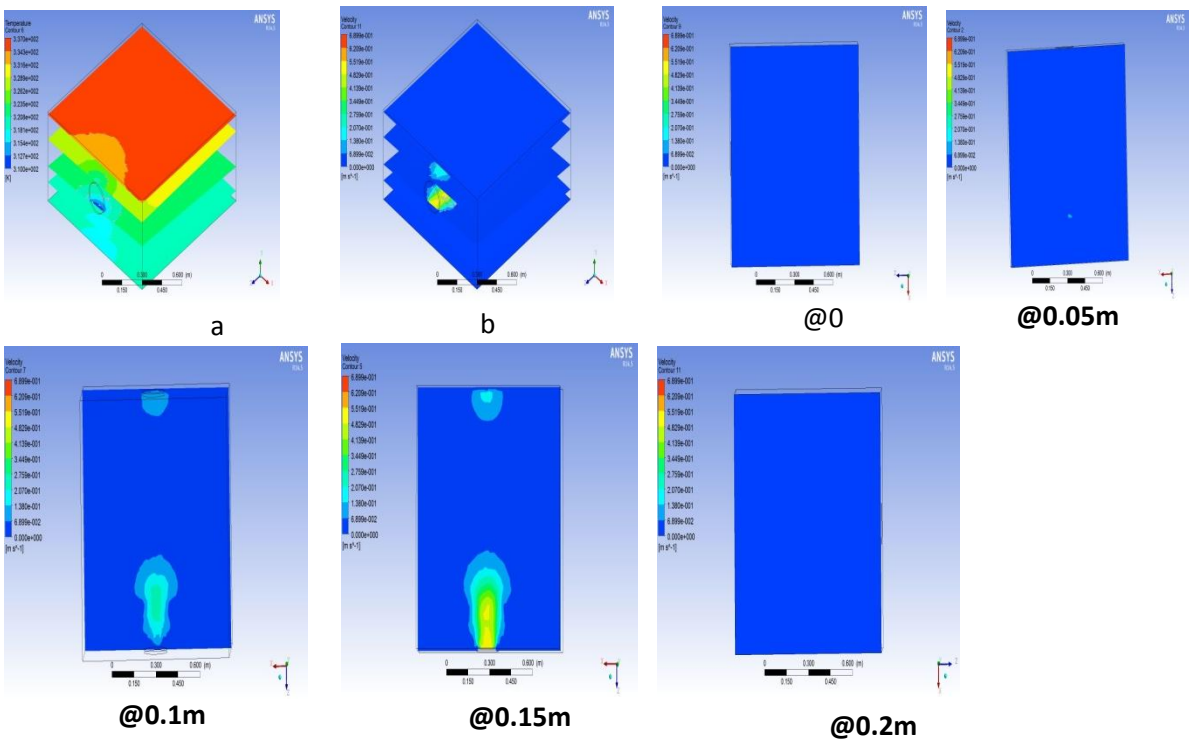

Figure 8. Effect of tray position on air and temperation distribution contour, a: Temperature distribution Contours for different tray positions, b: stack airflow distribution contours.

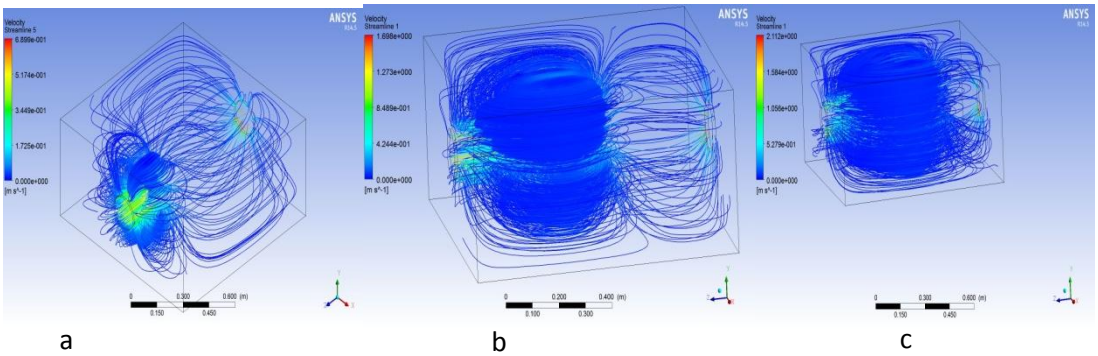

Figure 9. Effect of airflow rate on air distribution pattern, a: Free convection streamline, b: Streamlines distribution at 1.2 m/s airflow speed, c: Streamline distribution at 1.5 m/s airflow speed.

This reveals that though the *Re* of fluid flow within the simulated dryer increases with increase in airflow speed, the airflow remains stable and laminar within the considered dryer length. All the streamline paths converge at exit of the outlet vent. This suggests the possibility of effective removal of moisture from the dryer to the immediate environment.

Effect of collector inclination on temperature distribution

Collector inclination angle is necessary to obtain maximum irridiation. Fig.10 shows the contour of solar heat flux received within flat plate solar collector at inclination angle 0˚. The contour reveals east-west traveling direction of solar irriadiation. Fig. 10 shows the contour of temperature within the drying chamber due to the receipt of solar irridation on the flat plate solar collector of different angles of inclination. The contour reveals uneven distribution of solar heat flux within drying chamber. This numerically showed that amount of solar irridation received by the solar collector is a function of latitude of research location and inclination angle. This is in line with recommendation obtainable in literatures (Gbaha et al., 2007; Amer et al., 2015).

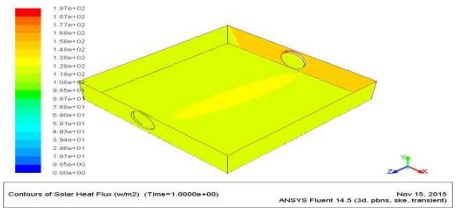

Solar heat flux at angle 0˚

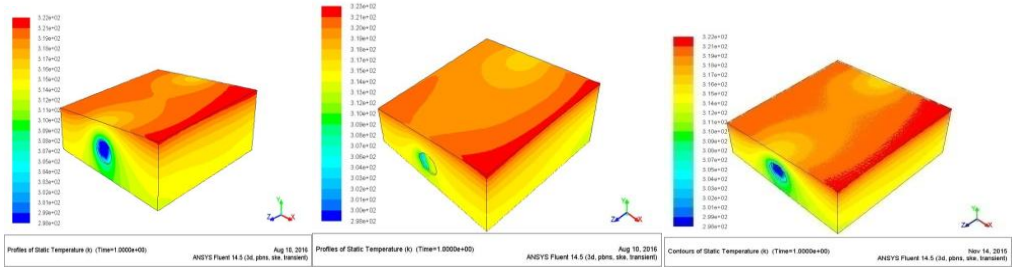

Angle 7.5˚ Angle 12˚ Angle

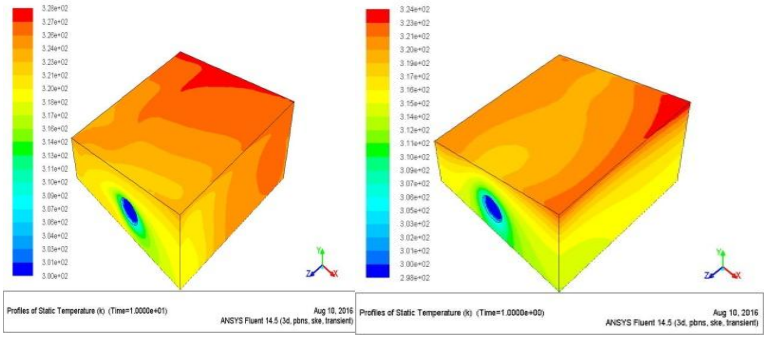

Angle 15˚ Angle 14˚

Fig. 10: Contours of solar heat flux and temperature distribution within drying chamber using varied inclination angle

Since maximum solar heat flux is obtainable within solar collector range of (α - 10) ≤ β ≥ (α + 10) according to Gbaha et al. (2007) analytical based recommendation, different angles within the recommended range were simulated. The contours of the temperature distribution with respect to solar collector angle are shown (Fig. 10) and the values of it average temperatur within

the drying chamber are shown in (Fig. 11). From (Fig. 11), optimum solar energy is obtainable at collector inclination angle 14˚. This angle corresponds to angle ranges (α-6.5) ≤ β ≥ (α+6.5) of the earth polar system. This narrows analytical collector inclination angel range, and the modified range can be computed and simulated using any global polar positioning elsewhere.

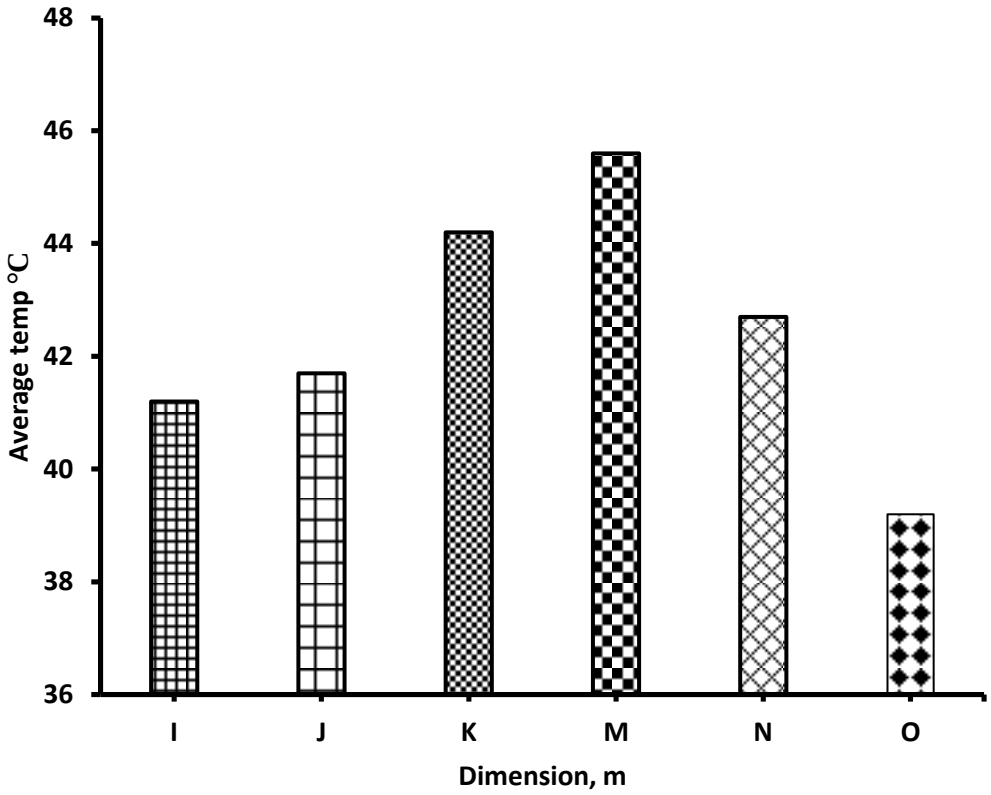

Figure 11. Average temperature within drying chamber with respect to varied inclination angles.

Mixed-mode solar dryer CFD and experimental result comparison

The simulated results from CFD of the model dryer were compared to the results from experimental runs as well as data from (Fagunwa et al., 2009). Figures 12 showed the plot of the numerical and experimental comparisons. Figure 12a showed CFD results compared with the experimental data in this work, and figure 12b showed comparison of CFD and experimental results of the Fagunwa's mixed-mode solar dryer for cocoa beans. Base on the model dryer, the figure 12a revealed that the dryer temperatures obtained using CFD and experimentation compare with good agreement. For the same dryer, air temperature ranges between 29.1 to 78 ˚C were observed for CFD, and the corresponding temperature range obtained through experimentation were 33.9 to 77 ˚C. However, a significant discrepance in CFD and experimental results were observed in figure 12b, and figure 12b was based on results obtained through Fagunwa's model dryer using CFD and experimental parameters. Unlike the model dryer in this work, the figure 12b revealed that CFD results of the Fagunwa's dryer were higher than temperature (31 – 54 ˚C) obtained through experimentation using the dryer.

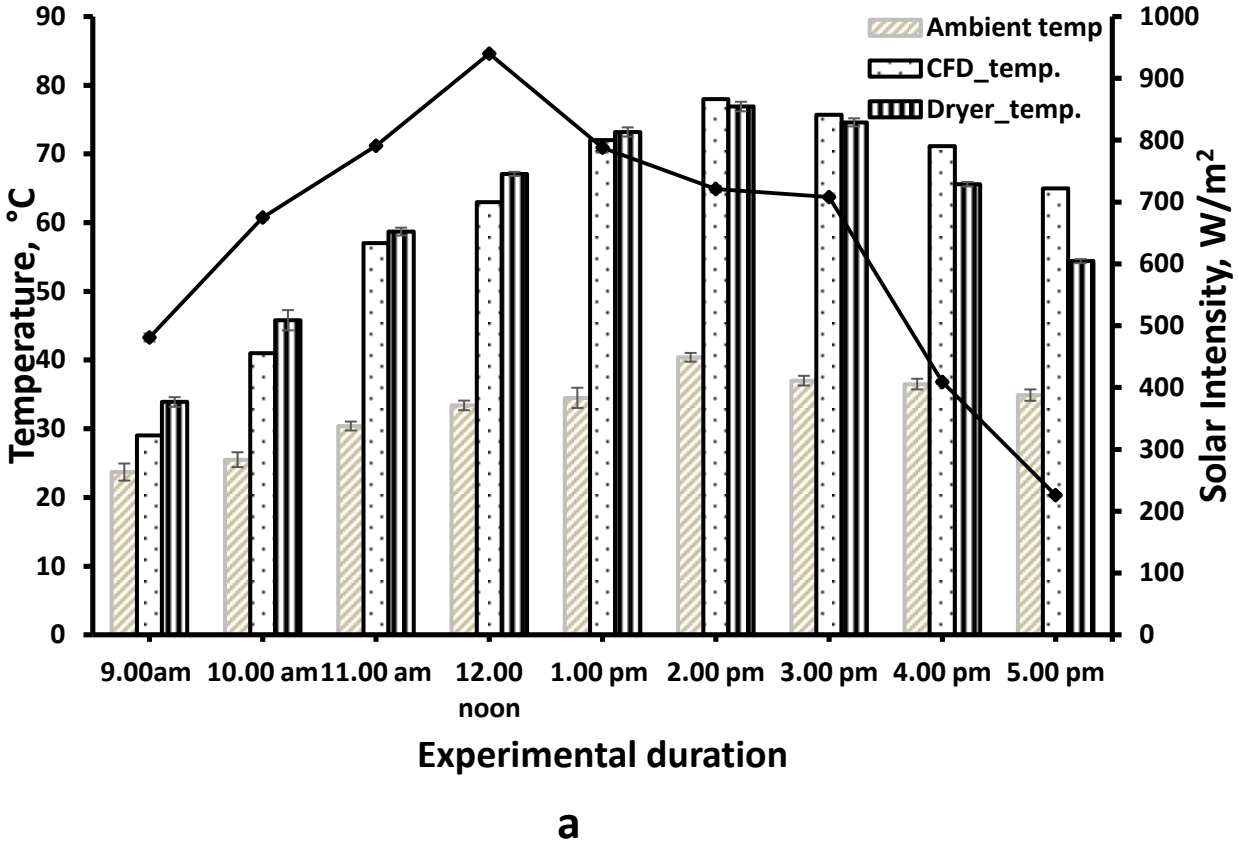

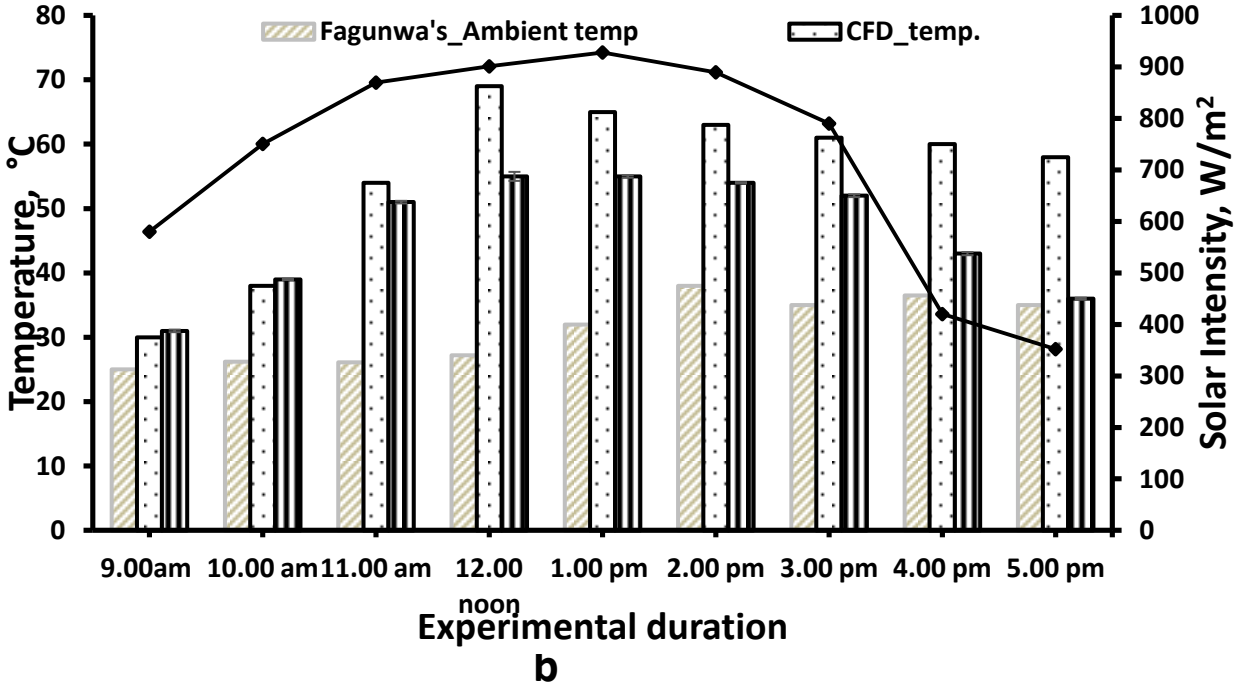

Figure 12: Comparison of air temperature from (a) CFD and experimental data; (b) CFD and Fagunwa's et al

CONCLUSION

In conclusion, numerical modelling of mixed-mode solar dryers could be a good approach to maximizing solar drying systems for thermal output and reduce long drying times and improving drying quality. Drying chamber of different dimensions were simulated using ANSYS software version 14.5. drying surface area, drying bed height, collector inclination angle based on latitude of research location and air flowspeed as well as drying tray positions were varied and simulated for optimal performance. The numerical model dryer was compared using numerical and experimental method. The simulation boundary conditions for comparison were based on the experimental conditions in this work and the one found in similar dryer type for cocoa beans. The numerical results shows that temperature obtained inside the chamber increases with increase in exposed surface area of collector. A step increament of 3 ˚C were recorded for every 0.1 m^2 increament in exposed surface area. The temperarture obtained inside collector decreases with decrease in collector depth with typical temperature decrease of 1.5 ˚C for every 0.1 m increament in height. Optimal collector inclination angle is obtainable at angle 14˚. This narrow the analytical-based wide range of collector inclination angle recommeded in literatures to (α-6.5) ≤ β ≥ (α+6.5) of the earth polar system. The temperature obtained using CFD model and experimental dryer compared with good fit, and a considerable improvement in numerical model dryer was observed over the existing analytically modelled dryer.

ACKNOWLEDGEMENT

This work was supported by Africa Centre of Excellence in ICT-Driven Knowledge Park (OAK-PARK), a World Bank initiative.

Nomenclature

A	Apparent Solar irradiation (wm^{-2})
A_c	Collector area (m^2),
A_s	Surface area of the collector (m^2
$C_{1\epsilon}$, $C_{2\epsilon}$, $C_{3\epsilon}$	Dissipated heat constant
c	Specific heat (kJ $kg^{-1}K^{-1}$)
CFD	Computational fluid dynamic
E_{dn}	Normal direct irradiation
F	Sum of body force (N)
F_r	Heat removal factor
h	Convective heat transfer (kW$\mathrm{m}^2\mathrm{K}^{-1}$)
h_{tot}	Total specific enthalpy
I	Apparent solar irradiation
$\mathrm{I}_{\mathrm{tot}}$	Total incident radiation (Wm^{-2})
K	kinetic energy (J)
k	Thermal conductivity (W$m^{-1}\mathrm{K}^{-1}$)
$\dot{\mathrm{M}}$	Mass flow rate (kgm^{-1}).
Mc	Moisture content
M_e	Equilibrium moisture content
MR	Moisture ratio
M_s	Mass of dry beans
M_{w}	Mass of water
P	Modified pressure (Pa)

P_b	Generation of turbulence kinetic energy due to buoyancy (J)
P_k	Generation of turbulence kinetic energy due to the mean velocity gradients (J)
Q_r	Radiant energy (J)
S_ϵ, S_k	Solar energy source (J)
T	Temperature (˚C)
t	Time, s
T_a	Ambient air temperature (K)
T_c	Expected average temperature of the air below the bed and the collector's absorber (K)
T_D	Expected average temperature of air above the bed (K)
u	Relative velocity (ms^{-1})
Ui (U, V, W)	Velocity component (ms^{-1})
v	Volume (m^3)
wb	wet basis
xi (x, y, z)	Cartesian coordinate (m)
Y_M	Fluctuating dilatation in compressible
	Turbulence

Symbols

ρ_y	Absorptivity
θ	Atmospheric extinction coefficient
ρ	Density (kgm^{-3})
μ_{eff}	Effective viscosity (kg$m^{-1}s^{-1}$)
β	Inclination angle
α	Latitude of a location (˚)
σ_k	Prandtl number
∈	Rate of dissipation of turbulent kinetic
	Energy (m^2s^{-3})
$\propto_y$	Reflectivity
τ_y	Transmissivity
ɾ	Transmittance (Wm^{-2})
μ_t	Turbulent viscosity (kg$m^{-1}s^{-1}$)
μ	Viscosity (kg$m^{-1}s^{-1}$)

Subscripts

dv- Directly-visible

di - Direct irradiation;

dh - Diffuse hemispherical components

REFERENCES

Aboul-Enein, S., El-Sebaii, A., Ramadan, M., & El-Gohary, H. (2000). Parametric study of a solar air heater and without thermal storage for solar drying applications. Renewable energy, 21(3-4), 505-522.

Adeniyi, A. A., Mohammed, A., & Aladeniyi, K. (2012). Analysis of a solar dryer box with ray tracing CFD technique. International Journal of Scientific & Engineering Research, 3(10),1-5.

Amer, B., Hossain, M., & Gottschalk, K. (2010). Design and performance evaluation of a new hybrid solar dryer for banana. Energy conversion and management, 51(4), 813-820.

ASHRAE. (2009). American Society of Heating, Refrigerating Air-Conditioning Engineers (ASHRAE) Handbook of Fundamentals. Inc.: Atlanta, GA, USA.

AusAID. (2010). Cocoa Processing Methods for the Production of High Quality Cocoa in Vietnam. Australian Government Retrieved from https://www.academia.edu/26982960/Cocoa_fermentation_manual_Vietnam.

El-Sebaii, A., & Shalaby, S. (2012). Solar drying of agricultural products: A review. Renewable and Sustainable Energy Reviews, 16(1), 37-43.

Engineering Tool Box. (2003). Thermal Conductivity of common Materials and Gases. [online].

Retrieved 5 May, 2016. Available at: https://www.engineeringtoolbox.com/thermal-conductivity-d_429.html

Fagunwa, A. O., Koya, O. A., & Faborode, M. O. (2009). Development of an intermittent solar dryer for cocoa beans. Agricultural Engineering International: CIGR Journal.

Fudholi, A., Sopian, K., Ruslan, M. H., Alghoul, M., & Sulaiman, M. (2010). Review of solar dryers for agricultural and marine products. Renewable and Sustainable Energy Reviews, 14(1), 1-30.

Gatea, A. A. (2010). Design, construction and performance evaluation of solar maize dryer. Journal of Agricultural Biotechnology and sustainable development, 2(3), 39-46.

Gbaha, P., Andoh, H. Y., Saraka, J. K., Koua, B. K., & Toure, S. (2007). Experimental investigation of a solar dryer with natural convective heat flow. Renewable energy, 32(11), 1817-1829.

Hodali, R., & Bougard, J. (2001). Integration of a desiccant unit in crops solar drying installation: optimization by numerical simulation. Energy Conversion and Management, 42(13), 1543-1558. doi:https://doi.org/10.1016/S0196-8904(00)00159-X

Ingle, P., Pawar, A., Deshmukh, B., & Bhosale, K. (2013). CFD analysis of solar flat plate collector. International Journal of Emerging Technology and Advanced Engineering, 3(4), 337-342.

Jain, D., & Jain, R. K. (2004). Performance evaluation of an inclined multi-pass solar air heater with in-built thermal storage on deep-bed drying application. Journal of Food Engineering, 65(4), 497-509.

Jairaj, K. S., Singh, S. P., & Srikant, K. (2009). A review of solar dryers developed for grape drying. Solar energy, 83(9), 1698-1712. doi:https://doi.org/10.1016/j.solener.2009.06.008

Jones, W., & Launder, B. E. (1972). The prediction of laminarization with a two-equation model of turbulence. International journal of heat and mass transfer, 15(2), 301-314.

Kumar, M., Sansaniwal, S. K., & Khatak, P. (2016). Progress in solar dryers for drying various commodities. Renewable and Sustainable Energy Reviews, 55, 346-360. doi:https://doi.org/10.1016/j.rser.2015.10.158

Maia, C. B., Ferreira, A. G., Cabezas-Gómez, L., Hanriot, S. D. M., & Martins, T. D. O. (2012). Simulation of the airflow inside a hybrid dryer. International Journal of Research and Reviews in Applied Sciences, 10(3), 382-389.

Markatos, N. (1983). Heat Transfer, xiii, 2nd edn., BV Karlekar, RM Desmond. West Publishing Co., St. Paul, Minnesota (1982),+ 799 pp.+ solutions manual, 417 pp: Pergamon.

Simate, I. (2003). Optimization of mixed-mode and indirect-mode natural convection solar dryers. Renewable energy, 28(3), 435-453.

Singh, S., & Kumar, S. (2012). Testing method for thermal performance-based rating of various solar dryer designs. Solar energy, 86(1), 87-98.